

Examining exotic structure of proton-rich nucleus ^{23}Al

D. Q. Fang*,¹ W. Guo,¹ C. W. Ma,¹ K. Wang,¹ T. Z. Yan,¹ Y. G. Ma,¹ X. Z. Cai,¹ W. Q. Shen,¹ Z. Z. Ren,² Z. Y. Sun,³ J. G. Chen,¹ W. D. Tian,¹ C. Zhong,¹ M. Hosoi,⁴ T. Izumikawa,⁵ R. Kanungo,⁶ S. Nakajima,⁴ T. Ohnishi,⁷ T. Ohtsubo,⁵ A. Ozawa,⁸ T. Suda,⁷ K. Sugawara,⁴ T. Suzuki,⁴ A. Takisawa,⁵ K. Tanaka,⁷ T. Yamaguchi,⁴ and I. Tanihata⁶

¹Shanghai Institute of Applied Physics, Chinese Academy of Sciences, Shanghai 201800, People's Republic of China

²Department of Physics, Nanjing University, Nanjing 210008, People's Republic of China

³Institute of Modern Physics, Chinese Academy of Sciences, Lanzhou 730000, People's Republic of China

⁴Department of Physics, Saitama University, Saitama 338-8570, Japan

⁵Department of Physics, Niigata University, Niigata 950-2181, Japan

⁶TRIUMF, 4004 Wesbrook Mal, Vancouver, British Columbia, V6T 2A3, Canada

⁷Institute of Physical and Chemical Research (RIKEN), Wako-shi, Saitama 351-0198, Japan

⁸Institute of Physics, University of Tsukuba, Ibaraki 305-8571, Japan

(Dated: November 2, 2018)

The longitudinal momentum distribution ($P_{//}$) of fragments after one-proton removal from ^{23}Al and reaction cross sections (σ_R) for $^{23,24}\text{Al}$ on carbon target at 74A MeV have been measured. The $^{23,24}\text{Al}$ ions were produced through projectile fragmentation of 135A MeV ^{28}Si primary beam using RIPS fragment separator at RIKEN. $P_{//}$ is measured by a direct time-of-flight (TOF) technique, while σ_R is determined using a transmission method. An enhancement in σ_R is observed for ^{23}Al compared with ^{24}Al . The $P_{//}$ for ^{22}Mg fragments from ^{23}Al breakup has been obtained for the first time. FWHM of the distributions has been determined to be 232 ± 28 MeV/c. The experimental data are discussed by using Few-Body Glauber model. Analysis of $P_{//}$ demonstrates a dominant d -wave configuration for the valence proton in ground state of ^{23}Al , indicating that ^{23}Al is not a proton halo nucleus.

PACS numbers: 25.60.-t, 21.60.-n, 27.30.+t

Since the pioneering measurements of interaction cross sections (σ_I) and observation of a remarkably large σ_I for ^{11}Li [1, 2], exotic structures like neutron halo or skin in light neutron-rich nuclei have been found. Experimental measurements of reaction cross section (σ_R), fragment momentum distribution ($P_{//}$) after one or two nucleons removal, quadrupole moment and Coulomb dissociation have been demonstrated to be very effective methods to investigate nuclear halo structure. The neutron skin or halo nuclei $^{6,8}\text{He}$, ^{11}Li , ^{11}Be , ^{19}C etc. [1, 2, 3, 4, 5, 6, 7], have been identified by these experimental methods. Due to Coulomb barrier, identification of a proton halo is more difficult compared to a neutron halo. The quadrupole moment, $P_{//}$ and σ_R data indicate a proton halo in ^8B [8, 9, 10, 11, 12], whereas no enhancement is observed in the measured σ_I at relativistic energies [13]. The proton halo in $^{26,27}\text{P}$ and ^{27}S has been predicted theoretically [14, 15]. Measurements of $P_{//}$ have shown a proton halo character in $^{26,27,28}\text{P}$ [16].

Proton-rich nucleus ^{23}Al has a very small separation energy ($S_p = 0.125$ MeV) [17] and is a possible candidate of proton halo. An enhanced σ_R for ^{23}Al has been observed in a previous experiment [18, 19]. To reproduce the σ_R for ^{23}Al within framework of Glauber model, a dominating $2s_{1/2}$ component for the valence proton is shown [18]. A long tail in proton density distribution

has been extracted for ^{23}Al which indicated halo structure. The spin and parity (J^π) for ground state of ^{23}Al has been deduced to be $5/2^+$ in a recent measurement of magnetic moment [20]. This result favors a d -wave configuration for the valence proton in ^{23}Al . But it does not eliminate the possibility of a s -wave valence proton if its ^{22}Mg core is in excited state. Therefore it will be very important to determine configuration of the valence proton for ^{23}Al . As we know, $P_{//}$ of the fragment carries structure information of the projectile. However, there are no such experimental data for ^{23}Al up to now. In this paper we will report simultaneously measurements of σ_R and $P_{//}$ for ^{23}Al and also σ_R for ^{24}Al .

The experiment was performed at the RIKEN Projectile fragment Separator (RIPS) in RIKEN Ring Cyclotron Facility. The experimental setup is shown in Fig. 1. Secondary beams were generated by fragmentation reaction of 135A MeV ^{28}Si primary beam on a ^9Be production target in F0 chamber. In the dispersive focus plane F1, an Al wedge-shaped degrader (central thickness; 583.1 mg/cm², angle; 6 mrad) was installed. A delay-line readout Parallel Plate Avalanche Counter (PPAC) was placed to measure the beam position. Then the secondary beam was directed onto the achromatic focus F2. Two delay-line readout PPACs were installed to determine the beam position and angle. An ion chamber ($200\phi \times 780\text{mm}$) was used to measure energy loss (ΔE) of the secondary beams [21]. An ultra-fast plastic scintillator (0.5 mm thick) was placed before a carbon reaction target (377 mg/cm² thick) to measure time-of-flight (TOF) from the

*Corresponding author. Email: dqfang@sinap.ac.cn

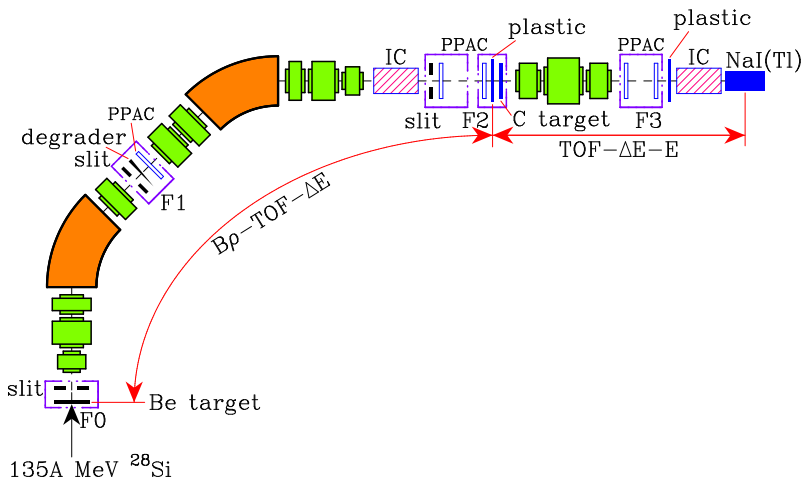


FIG. 1: (Color online) Experimental setup at the fragment separator RIPS.

PPAC at F1. The particle identification before the reaction target was done by means of $B\rho-\Delta E$ -TOF method.

After the reaction target, a quadrupole triplet was used to transport and focus the beam onto F3 (~ 6 m from F2). Two delay-line readout PPACs were used to monitor the beam size and emittance angle. Another plastic scintillator (1.5 mm thick) gave a stop signal of the TOF from F2 to F3. A smaller ion chamber ($90\phi \times 650\text{mm}$) was used to measure energy loss (ΔE) of the beam. Total energy (E) was measured by a NaI(Tl) detector. The particles were identified by TOF- ΔE - E method. An example of typical particle identification spectra at F3 for the fragment from ^{23}Al breakup is shown in Fig. 2. In this spectrum, fragments with different nuclear charge were already subtracted by TOF and ΔE method.

Under assumption of a sudden valence-nucleon removal, the momentum distribution of fragments can be used to describe that of the valence proton. The $P_{//}$ of fragments from breakup reactions was determined from the TOF between the two plastic scintillators installed at F2 and F3. Position information measured by the PPAC at F1 was used to derive incident momentum of the beam.

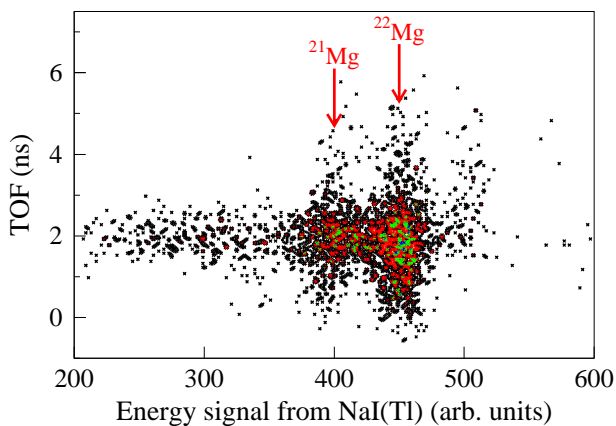


FIG. 2: (Color online) Particle identification at F3 by the bidimensional plot between TOF from F2 to F3 and energy signal from NaI(Tl) (corrected with TOF).

The momentum of fragment relative to the incident projectile in laboratory frame was transformed into that in the projectile rest frame using Lorentz transformation.

In order to estimate and subtract reactions of the projectile in material other than the carbon target, measurements without the reaction target were also performed and the beam energy was reduced by an amount corresponding to the energy loss in the target. For one-proton removal reactions of ^{23}Al , this background was carefully reconstructed and subtracted based on ratio of fragments to unreacted projectile identified in the target-out measurement and also broadening effect of the carbon target on $P_{//}$. The obtained momentum distribution of ^{22}Mg fragments from ^{23}Al breakup in the carbon target at 74A MeV is shown in Fig. 3. We normalized experimental counts to the measured one-proton removal cross section (σ_{-1p}) so that $\sum N(p_i)\Delta p_{//}$ equals σ_{-1p} . A Gaussian function was used to fit the distributions. The full width at half maximum (FWHM) was determined to be 232 ± 28 MeV/c after unfolding the Gaussian-shaped system resolution (41 MeV/c). The FWHM is consistent with Goldhaber model's prediction (FWHM=212 MeV/c with $\sigma_0 = 90$ MeV/c) within the error bar [22]. Since magnetic fields of the quadrupoles between F2 and F3 were optimized for the projectile in the measurement, momentum dependence of transmission from F2 to F3 for fragments was simulated by the code MOCADI [23]. The effect of transmission on the width of $P_{//}$ distribution was found to be negligible which is similar with the conclusion for neutron-rich nuclei [24, 25]. Using the estimated transmission value, the one-proton removal cross sections for ^{23}Al was obtained to be 63 ± 9 mb.

Reaction cross section is determined using the transmission method:

$$\sigma_R = \frac{1}{t} \ln \left(\frac{\gamma_0}{\gamma} \right) \quad (1)$$

where γ and γ_0 denote ratio of unreacted outgoing and incident projectiles for target-in and target-out cases, respectively; t thickness of the reaction target, i.e., number of particle per unit area.

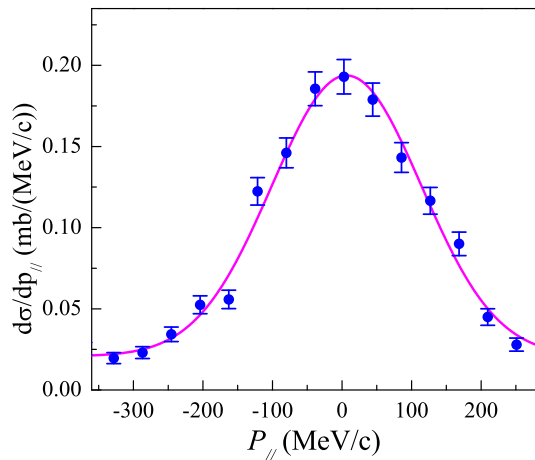


FIG. 3: (Color online) $P_{//}$ distribution of fragment ^{22}Mg after one-proton removal from ^{23}Al . The closed circles with error bars are the present experimental data, the solid curve is a Gaussian fit to the data.

The σ_R of $^{23,24}\text{Al}$ at 74A MeV were obtained to be 1609 ± 79 mb and 1527 ± 60 mb, respectively. The errors include statistical and systematic uncertainties. Probability of inelastic scattering reaction was estimated to be very small ($< 1\%$), e.g., the inelastic cross section is only around 11 mb for ^{23}Al which is much smaller than the error of σ_R .

Results of previous and current experiments are shown in Fig. 4. Since the energy is different in two experiments, the previous σ_R data at $\sim 30A$ MeV [18] were scaled to the present energy (74A MeV) using a phenomenological formula [26]. First the radius parameter (r_0) in this formula was adjusted to reproduce the σ_R at $\sim 30A$ MeV, then the same r_0 was used to calculate the σ_R at 74A MeV. As shown in Fig. 4, the σ_R of $^{23,24}\text{Al}$ from present and previous experiments are in good agreement. And we observed a small enhancement in σ_R for ^{23}Al in our data again.

To interpret the measured reaction cross sections and momentum distributions, we performed a Few-Body Glauber model (FBGM) analysis for $P_{//}$ of $^{23}\text{Al} \rightarrow ^{22}\text{Mg}$ processes and σ_R of $^{23,24}\text{Al}$ [27, 28, 29]. In this model, a core plus proton structure is assumed for the projectile. The total wavefunction of the nucleus is expressed as

$$\Psi = \sum_{ij} \psi_{\text{core}}^i \phi_0^j, \quad (2)$$

where ψ_{core} and ϕ_0 are wavefunctions of the core and valence proton; i, j denote different configurations for the core nucleus and valence proton, respectively. For the core, harmonic oscillator (HO) functions were used for the density distributions. The wavefunction of the valence proton was calculated by solving the eigenvalue problem in a Woods-Saxon potential. The separation energy of the last proton is reproduced by adjusting the potential depth. In the calculation, the diffuseness and

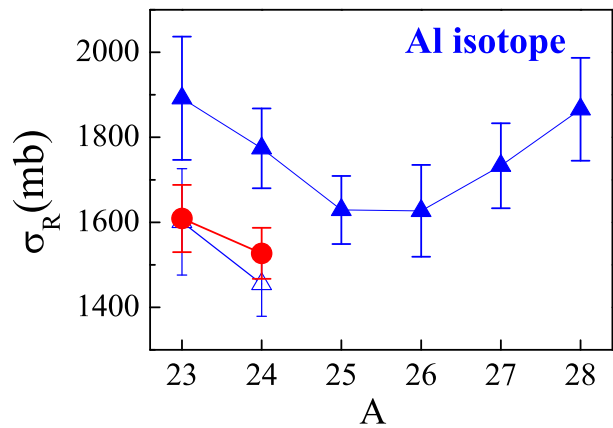


FIG. 4: (Color online) The mass dependence of σ_R for Al isotopes. The solid circles are results of the present experiment ($E = 74A$ MeV), the solid triangles are the previous experimental data ($E \sim 30A$ MeV) [18], and the open triangles are the previous data scaled to 74A MeV.

radius parameter were chosen to be 0.67 fm and 1.27 fm, respectively [24].

In the recent g -factor measurement using a β -NMR method, the spin and parity for ground state of ^{23}Al is shown to be $5/2^+$. It gives a strong restriction on the possible structure of this nucleus. Assuming $^{22}\text{Mg}+p$ structure, three most probable configurations for $J^\pi = 5/2^+$ of ^{23}Al are: $0^+ \otimes 1d_{5/2}$, $2^+ \otimes 1d_{5/2}$ and $2^+ \otimes 2s_{1/2}$ [20]. The s -wave configuration is therefore possible for the core in the excited state.

The momentum distributions for the valence proton in s or d -wave configuration are calculated by using FBGM. In this calculation, the parameters α and σ_{NN} in the profile function $\Gamma(b) = \frac{1-i\alpha}{4\pi\beta^2} \sigma_{NN} \exp(-\frac{b}{2\beta^2})$ (b is the impact parameter) are taken from Ref. [28]. The range parameter (β) is calculated by the formula which is determined by fitting the σ_R of $^{12}\text{C} + ^{12}\text{C}$ from low to relativistic energies [30]. β is 0.35 fm at 74A MeV. To fix the core size, the width parameters in the HO density distribution of ^{22}Mg were adjusted to reproduce the experimental σ_I data at around 1A GeV [31]. The extracted effective root-mean-square matter radius ($R_{\text{rms}} \equiv \langle r^2 \rangle^{1/2}$) for ^{22}Mg is 2.89 ± 0.09 fm. To see the separation energy dependence, the FWHM of $P_{//}$ is determined assuming an arbitrary separation energy in calculation of the wavefunction for the valence proton in ^{23}Al and shown in Fig. 5. If we adopt a larger radius of $R_{\text{rms}} = 3.6$ fm for ^{22}Mg to see the core size effect on $P_{//}$, we obtained solid and open squares of FWHM in Fig. 5. The one proton separation energies for ^{22}Mg in the ground and excited ($J^\pi = 2^+$, $E_x = 1.25$ MeV) states are taken as 0.125 MeV and 1.375 MeV ($E_x + 0.125$ MeV). Those two values are marked by two arrows in Fig. 5. In this figure, we can see that the width for the s and d -wave are obviously separated. The width for the s -wave is much lower than the experimental data, while that of the d -wave is close to the experimental FWHM. With the increase of

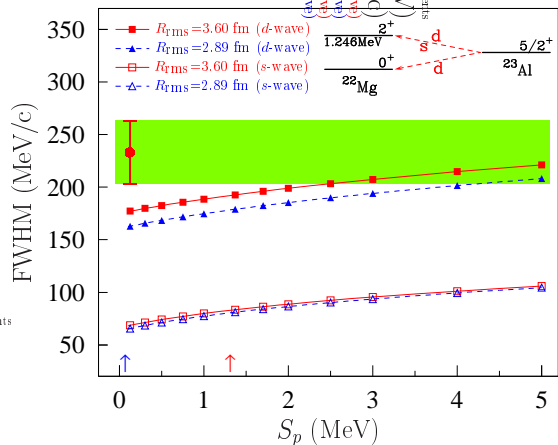


FIG. 5: (Color online) The dependence of FWHM for the $P_{//}$ distribution after one-proton removal of ^{23}Al on the separation energy of the valence proton. The solid circles with error bars is result of the present experiment, the shaded area refers to error of the data. The solid and open squares are the FBGM calculations for the d and s -wave configuration of the valence proton with the core $R_{\text{rms}} = 3.6$ fm. The solid and open triangles are for the core $R_{\text{rms}} = 2.89$ fm. The lines are just for guiding the eyes. The two arrows refer to the separation energy of 0.125 MeV and 1.37 MeV (the excitation energy for the first excited state of ^{22}Mg plus the experimental one proton separation energy of ^{23}Al).

S_p , the width of $P_{//}$ increases slowly. It means that $P_{//}$ will become wider for ^{22}Mg in the excited state. The effect of the core size on $P_{//}$ is negligible for the s -wave and small for the d -wave configuration. The larger sized core will give a little wider $P_{//}$ distribution. From comparison of the FBGM calculation with the experimental data in Fig. 5, it is clearly shown that the valence proton in ^{23}Al is dominantly in the d -wave configuration. The possibility for the s -wave should be very small. Furthermore, it is possible to have an excited core inside ^{23}Al . This is consistent with the shell model calculations and also the Coulomb dissociation measurement [20, 32].

From above discussions of $P_{//}$, the valence proton in ^{23}Al is determined to be in the d -wave configuration, which is used in the following calculations. In the calculation of σ_R for ^{23}Al using the FBGM, at first $R_{\text{rms}} = 2.89 \pm 0.09$ fm is used for its ^{22}Mg core by reproducing the σ_I data as described above. But the calculated σ_R is much lower than the obtained σ_R data. One reason may be due to the global underestimation of σ_R found at intermediate energies in the Glauber model [33]. Different method has been tried to correct this problem [4, 30, 34]. These corrections are performed for almost light stable nuclei. The σ_R of ^{24}Al is calculated with the size of its ^{23}Mg core determined by fitting σ_I at around 1A GeV [31]. But the calculated σ_R for ^{24}Al is only 1430 mb which is $\sim 10\%$ lower than the present data. It was shown that scope of the discrepancy between the Glauber model calculation and experimental data is large even for stable nuclei [33]. To correct the

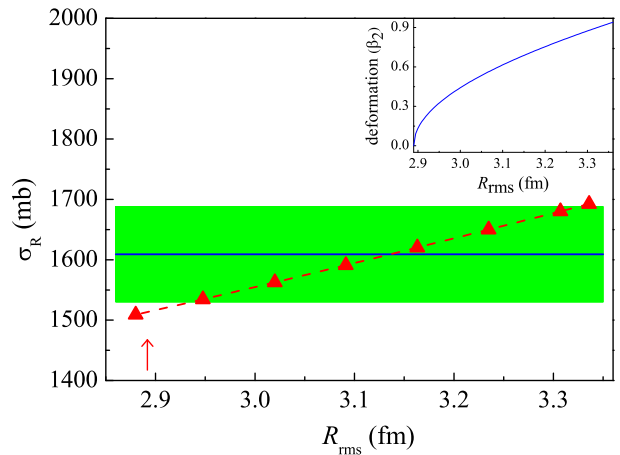


FIG. 6: (Color online) The dependence of σ_R at 74A MeV on the core size (R_{rms}). The horizontal line is the experimental σ_R value, the shadowed area is the error of σ_R . The triangles denote the FBGM calculations. The size of ^{22}Mg obtained by fitting the σ_I data at around 1A GeV is marked by an arrow. The inset shows the relationship between the quadrupole deformation parameter (β_2) and size of the core, for details see the text.

possible underestimation for nuclei with $A > 20$, we adjusted the range parameter to fit the σ_R of ^{24}Al from the present measurement. And $\beta = 0.8$ fm is obtained when the σ_R of ^{24}Al at 74A MeV is reproduced. Using this range parameter, the calculated σ_R value of ^{23}Al is still smaller than the data. Similar puzzle is also encountered for some neutron-rich nuclei. The large σ_I cannot be reproduced by the FBGM even for the valence neutron in the s -wave for ^{19}C and ^{23}O . One way is to enlarge the core size to reproduce the experimental σ_R [35, 36]. Here we changed the core size by adjusting width parameters in the HO density distribution of ^{22}Mg . The dependence of σ_R for ^{23}Al on the core size is calculated and shown in Fig. 6. The calculated results indicate that the core size is 3.13 ± 0.18 fm when the experimental σ_R data of ^{23}Al is reproduced ($8 \pm 7\%$ larger than the size of the bare ^{22}Mg nucleus).

In order to reproduce the σ_R of ^{23}Al from the current work, a larger sized core is deduced within the framework of the spherical Glauber model. It should be pointed out that this enlarged core may not necessarily reflect increased physical size of the nucleus. The negligence of some specific effects in the Glauber model could lead to the larger sized core. The possible reasons for the enlargement will be discussed qualitatively below. The effect of quadrupole deformation (β_2 , the parameter describing the deformation) on the rms radius can be expressed as $R_{\text{rms}}^{\beta_2} = \sqrt{(1 + \frac{5}{4\pi}\beta_2^2)} R_{\text{rms}}^{\beta_2=0}$ [37]. As shown in the inset of Fig. 6, R_{rms} of the core changes quickly with the increase of β_2 . This simple relationship between R_{rms} and β_2 indicates that a deformed core inside ^{23}Al will give a larger sized ^{22}Mg . In order to reproduce the σ_R of ^{23}Al , the lower limit of R_{rms} for the core is 2.95

fm as we can see from the calculated results in the figure. If we assume that the shape of ^{22}Mg as a nucleus is spherical and enlargement of the core is due to deformation, the lower limit of $\beta_2 = 0.3$ for the core could be deduced from the inset of Fig. 6. Deformation of $\beta_2 = 0.6$ will give around 8% larger radius for the ^{22}Mg core. The experimental and theoretical investigations have demonstrated the deformation for ^{22}Mg . The experimental β_2 is 0.566 [38], the calculated β_2 by RMF and generalized hybrid derivative coupling model are around 0.4 and 0.6, respectively [39, 40]. If the bare nucleus ^{22}Mg is deformed, the above analysis indicates that ^{22}Mg as a core in ^{23}Al may have larger deformation as compared with ^{22}Mg as a nucleus. Additionally, the first excited state of ^{22}Mg was calculated within the RMF framework and its R_{rms} is obtained to be around 2.4% larger than that of the ground state [41, 42]. Thus the core excitation effect may also contribute to the larger size for ^{22}Mg . As demonstrated by the shell model calculations, the configuration of ^{22}Mg (ground state) plus a d -wave proton is dominant in ^{23}Al [20]. If deformation and excitation effects exist in the core, the first one may be the main component.

In summary, the longitudinal momentum distribution of fragments after one-proton removal for ^{23}Al and reaction cross sections for $^{23,24}\text{Al}$ were measured. An enhancement was observed for the σ_R of ^{23}Al . The $P_{//}$ distributions were found to be wide and consistent with the Goldhaber model's prediction. The experimental $P_{//}$ and σ_R results were discussed within framework of the Few-

Body Glauber model. We determined the valence proton to be a dominant d -wave configuration in the ground state of ^{23}Al . It indicates no halo structure in this nucleus. But a larger sized ^{22}Mg core was deduced in order to explain both the σ_R and $P_{//}$ distributions within framework of the spherical Few-Body Glauber model. It is pointed out that deformation and core excitation effects may be two main reasons for the extracted larger sized core. Further theoretical investigations are needed to extract more specific structure information for ^{23}Al from the experimental data.

Acknowledgements

The authors are very grateful to all of the staff at the RIKEN accelerator for providing stable beams during the experiment. The support and hospitality from the RIKEN-RIBS laboratory are greatly appreciated by the Chinese collaborators. This work was partially supported by the National Natural Science Foundation of China (NNSFC) under Grant No. 10405032, 10535010, 10405033 and 10475108, Shanghai Development Foundation for Science and Technology under contract No. 06QA14062, 06JC14082 and 05XD14021, the Major State Basic Research Development Program in China under Contract No. 2007CB815004 and the Knowledge Innovation Project of Chinese Academy of Sciences under Grant No. KJCX3.SYW.N2.

-
- [1] I. Tanihata *et al.*, Phys. Rev. Lett. **55**, 2676 (1985).
 [2] I. Tanihata *et al.*, Phys. Lett. **B287**, 307 (1992).
 [3] I. Tanihata *et al.*, Phys. Lett. **B160**, 380 (1985).
 [4] M. Fukuda *et al.*, Phys. Lett. **B268**, 339 (1991).
 [5] D. Bazin *et al.*, Phys. Rev. Lett. **74**, 3569 (1995).
 [6] T. Nakamura *et al.*, Phys. Rev. Lett. **83**, 1112 (1999).
 [7] A. Ozawa *et al.*, Nucl. Phys. **A691**, 599 (2001).
 [8] T. Minamisono *et al.*, Phys. Rev. Lett. **69**, 2058 (1992).
 [9] W. Schwab *et al.*, Z. Phys. A **350**, 283 (1995).
 [10] R. E. Warner *et al.*, Phys. Rev. C **52**, R1166 (1995).
 [11] F. Negoita *et al.*, Phys. Rev. C **54**, 1787 (1996).
 [12] M. Fukuda *et al.*, Nucl. Phys. A **656**, 209 (1999).
 [13] M. M. Obuti *et al.*, Nucl. Phys. A **609**, 74 (1996).
 [14] B. A. Brown, P. G. Hansen, Phys. Lett. **B381**, 391 (1996).
 [15] Z. Z. Ren *et al.*, Phys. Rev. C **53**, R572 (1996).
 [16] A. Navin *et al.*, Phys. Rev. Lett. **81**, 5089 (1998).
 [17] G. Audi, A. H. Wapstra, Nucl. Phys. **A565**, 66 (1993).
 [18] X. Z. Cai *et al.*, Phys. Rev. C **65**, 024610 (2002).
 [19] H. Y. Zhang *et al.*, Nucl. Phys. **A707**, 303 (2002).
 [20] A. Ozawa *et al.*, Phys. Rev. C **74**, 021301R (2006).
 [21] K. Kimura *et al.*, Nucl. Inst. Meth. A **538**, 608 (2005).
 [22] A. S. Goldhaber, Phys. Lett. **B53**, 306 (1974).
 [23] N. Iwasa *et al.*, Nucl. Instrum. Methods B **126**, 284 (1997).
 [24] T. Yamaguchi *et al.*, Nucl. Phys. **A724**, 3 (2003).
 [25] D. Q. Fang *et al.*, Phys. Rev. C **69**, 034613 (2004).
 [26] W. Q. Shen *et al.*, Nucl. Phys. **A491**, 130 (1989).
 [27] Y. Ogawa *et al.*, Nucl. Phys. **A543**, 722 (1992).
 [28] Y. Ogawa *et al.*, Nucl. Phys. **A571**, 784 (1994).
 [29] B. Abu-Ibrahim *et al.*, Comput. Phys. Comm. **151**, 369 (2003).
 [30] T. Zheng *et al.*, Nucl. Phys. **A709**, 103 (2002).
 [31] T. Suzuki *et al.*, Nucl. Phys. **A630**, 661 (1998).
 [32] T. Gomi *et al.*, Nucl. Phys. **A758**, 761c (2005).
 [33] A. Ozawa *et al.*, Nucl. Phys. **A608**, 63 (1996).
 [34] M. Takechi *et al.*, Eur. Phys. J. A **25**, s01, 217 (2005).
 [35] R. Kanungo *et al.*, Nucl. Phys. **A677**, 171 (2000).
 [36] R. Kanungo *et al.*, Phys. Rev. Lett. **88**, 142502 (2002).
 [37] J. A. Christley, J. A. Tostevin, Phys. Rev. C **59**, 2309 (1999).
 [38] S. Raman *et al.*, At. Data Nucl. Data Tables **36**, 1 (1987).
 [39] G. A. Lalazissis *et al.*, Nucl. Phys. **A628**, 221 (1998).
 [40] Parna Mitra *et al.*, Phys. Rev. C **65**, 034329 (2002).
 [41] Z. Z. Ren *et al.*, Phys. Rev. C **57**, 2752 (1998).
 [42] J. G. Chen *et al.*, Eur. Phys. J. A **23**, 11 (2005).